Contents lists available at ScienceDirect

Applied Catalysis B: Environmental

journal homepage: www.elsevier.com/locate/apcatb

Photocatalytic splitting of thiols to produce disulfides and hydrogen over PtS/ZnIn$_2$S$_4$ nanocomposites under visible light

Lizhi Xu, Xiaoyu Deng, Zhaohui Li*

Research Institute of Photocatalysis, State Key Laboratory of Photocatalysis on Energy and Environment, College of Chemistry, Fuzhou University, Fuzhou, 350116, PR China

ABSTRACT

Photoreduction of $[PtCl_6]^{2-}$ over hexagonal ZnIn$_2$S$_4$ led to the formation of surface deposited small PtS nanoparticles with a size of ca. 3 nm. The resultant PtS/ZnIn$_2$S$_4$ nanocomposites were fully characterized and their performance for photocatalytic splitting of thiols to produce disulfides and hydrogen was investigated. It was found that PtS significantly promoted the photocatalytic performance for thiols splitting to produce disulfides and quantitative hydrogen over ZnIn$_2$S$_4$ under visible light and no over-oxidized products of thiols were produced. An optimum performance was observed over 0.5 wt% PtS/ZnIn$_2$S$_4$, with a complete transformation of thiols to disulfides in 6 h. PtS/ZnIn$_2$S$_4$ nanocomposite is stable during the photocatalytic reaction and can be easily separated for recycling. The photocatalytic thiols splitting over PtS/ZnIn$_2$S$_4$ is an efficient and cost effective strategy to produce disulfides, which exhibits 100% atom economy since hydrogen is generated concomitantly. This study demonstrates that the coupling of water reduction with organics oxidation over semiconductor-based photocatalysts may find great potentials in organic syntheses.

1. Introduction

The synthesis of disulfides has received extensive attention due to their indispensable roles in many important synthetic chemistry, biochemistry and industrial applications. The most common approach for the synthesis of disulfides is the oxidative coupling using stoichiometric oxidants or catalytic oxidation of thiols, since a number of thiols are commercially available or can be easily synthesized. However, over-oxidation of thiols to generate undesirable sulfoxides, sulfones, thiosulfinates or thiosulfonates as byproducts during the syntheses of disulfides from thiols occurs and therefore complicated purification processes are usually required [1,2]. In addition, sometimes hazardous chemicals and expensive metal containing reagents or catalysts are also involved [3–5].

With an effort to develop green and sustainable chemistry, recently researchers are paying increasing interest in the light-driven organic syntheses [6–10]. The use of light to trigger the transformation of thiols to produce disulfides is interesting considering that light has the unique capability of spatial control, which can induce reactions locally via delivering light to a specific area of interest, a capability especially important in biochemistry and catalysis. In 2010, Yoon et al. first reported that some light excitable aromatic thiols undergo photooxidative couplings to produce disulfides without the requirement of a catalyst

[11]. However, the substrate scope for this protocol is limited. The coupling of thiols to produce disulfides with concomitant generation of hydrogen was for the first time realized over a homogeneous [Mn (CO)$_5$Br] complex as the photosensitizer under UV irradiation [12]. More recently, Wu and co-workers reported that excellent conversion of thiols and high TON for the generation of disulfides can be achieved over CdSe QDs as photocatalyst using a high power Hg lamp [13]. As compared with the homogeneous catalysts, heterogeneous photocatalysts may provide more advantages in catalyst separation for recycling. Recently, heterogeneous photocatalysts GO-FePc (Pc = phthalocyanine) and CoOx-C,N@CeO$_2$ were also used in the oxidative coupling of thiols to produce disulfides using O$_2$ as oxidant [14,15]. Considering the atom efficiency, it is more desirable that the thiols can directly split to produce disulfides with concomitant generation of hydrogen.

Hexagonal ZnIn$_2$S$_4$ is a chalcogenide semiconductor that has a band gap corresponding to visible-light absorption as well as suitable band positions, with the top of its valance band located at 1.37 eV versus NHE, while the bottom of the conduction band located at –0.73 eV versus NHE [16]. ZnIn$_2$S$_4$ has been extensively studied for a series of photocatalytic applications under visible light [17–20]. When coupled with co-catalysts like Pt [21], MoS$_2$ [22,23], NiS [24] and RGO [25,26] to provide active sites and to lower the over potential for hydrogen

generation, $ZnIn_2S_4$ exhibit superior photocatalytic activity for hydrogen evolution in the presence of sacrificial agents like Na_2S/Na_2SO_3, TEA and TEOA [27–32].

Considering that thiols are also good electron donors and hydrogen sources, it is therefore interesting to investigate the photocatalytic splitting of thiols to form disulfides with the concomitant generation of hydrogen over $ZnIn_2S_4$. In this manuscript, we reported the deposition of PtS as a co-catalyst on the surface of $ZnIn_2S_4$ via a photo reduction process. The performance of the resultant $PtS/ZnIn_2S_4$ nanocomposites for photocatalytic splitting of thiols was investigated. Previous studies have revealed that metal chalcogenides like MoS_2 [33,34], WS_2 [35,36], NiS [37–39] and CoS [40,41] are active cocatalysts for photocatalytic H_2 evolution. It was found that PtS also acts as an efficient cocatalyst to promote photocatalytic thiols splitting to generate disulfides and quantitative hydrogen over $ZnIn_2S_4$ under visible light. This study not only provides an efficient, cost effective strategy for the production of disulfides, but also highlights the great potential of using semiconductor-based photocatalysts for light-driven organic syntheses by coupling with H_2O reduction to generate hydrogen.

2. Experimental

2.1. Preparations

All the reagents are analytical grade and used without further purifications. Hexagonal $ZnIn_2S_4$ was synthesized according to our previously reported method [42]. $PtS/ZnIn_2S_4$ nanocomposites were prepared via a photoreduction process. Typically, $ZnIn_2S_4$ (200 mg) was suspended in CH_3OH solution (3 mL) containing different amount of H_2PtCl_6. The resultant suspension was stirred under N_2 atmosphere for 30 min and irradiated with a 300 W Xe lamp. After illuminated for 3 h, the resultant products were filtered, washed with de-ionized water and dried overnight at 60 °C in oven. $PtS/ZnIn_2S_4$ nanocomposites with different amount of PtS were denoted as x wt% $PtS/ZnIn_2S_4$. For comparison, 1.0 wt% $Pd/ZnIn_2S_4$, 1.0 wt% $NiS/ZnIn_2S_4$ and 1.0 wt% $MoS_2/ZnIn_2S_4$ were prepared following the procedure reported previous [24,34].

2.2. Characterizations

X-ray diffraction (XRD) patterns were collected on a Rigaku Miniflex 600 X-ray diffractometer with Cu K_α radiation. X-ray photoelectron spectroscopy (XPS) measurements were performed on a PHI Quantum 2000 XPS system with a monochromatic Al K_α source and a charge neutralizer. All the binding energies were referred to the C 1 s peak at 284.6 eV of the surface adventitious carbon. The morphology of the sample was studied by a field emission scanning electron microscopy (SEM) (JSM-6700F). The transmission electron microscopy (TEM) and high-resolution transmission electron microscopy (HRTEM) images were measured using a JEOL model JEM 2010 EX instrument at an accelerating voltage of 200 kV. The powder particles were supported on a carbon film coated on a 3 mm diameter fine-mesh copper grid. A suspension of the sample in ethanol was sonicated and a drop was dripped on the support film. UV–vis diffraction spectra (UV–vis DRS) of the powders were obtained for the dry pressed disk samples using a UV–vis spectra photometer (Cary 500 Scan Spectrophotometers, Varian). $BaSO_4$ was used as a reflectance standard.

2.3. Photocatalytic reactions

The photocatalytic splitting of thiols to produce disulfides and hydrogen was performed in a schlenk tube. 5 mg of photocatalyst was evacuated and purged with N_2 for several times. A mixed solution of CH_3CN and H_2O in 3:1 (v/v) (2 ml) containing thiols (0.1 m mol) was pre-degassed with N_2 to remove any dissolved O_2 and was injected into the above schlenk tube. The suspension was irradiated with a 5 W LED

lamp (Light-emitting diodes, PCX50A, multichannel optical catalytic reaction system) with a wavelength centered at 450 nm. After reaction, the gaseous products were analyzed by GC-TCD (Shimadzu GC-2014) with a TDX-01 packed column. The filtrate was extracted with ethyl acetate for three times and was analyzed by GC-FID (Shimadzu GC-2014) equipped with a HP-5 capillary column. The apparent quantum yields (AQYs) for hydrogen evolution over 0.5 wt% $PtS/ZnIn_2S_4$ was measured under the same photocatalytic reaction condition except that a band pass filter centered at 420 nm was used. The AQYs for photocatalytic hydrogen production were represented as AQY % = (2 × number of hydrogen molecules formed) / (number of incident photons) × 100%.

3. Results and discussion

$ZnIn_2S_4$ was prepared according to our previously reported method, and different amounts of PtS were loaded on $ZnIn_2S_4$ by a photoreduction process. The XRD patterns of all the obtained products show 2θ peaks at values of 14.3, 21.2, 27.7, 30.4, 39.3, 47.5, 52.1, 55.8 and 76.4°, which can be assigned to (004), (006), (102), (104),(108), (110), (116), (022) and (123) crystallographic planes of hexagonal $ZnIn_2S_4$ phase (JCPDS 03-065-2023) (Fig. 1). No diffractions peaks corresponding to metallic Pt or Pt-containing compounds are observed in the XRD patterns of the products, probably due to the low amount of introduced Pt or the overlap of their diffractions peaks with those of hexagonal $ZnIn_2S_4$. However, the existence of Pt in the as-prepared products was confirmed by the XPS. The high resolution XPS spectra of the product in the Pt 4f region shows two peaks at 75.66 and 72.23 eV, which indicates that Pt exists as Pt^{2+} in the nanocomposite (Fig. 2a). The XPS spectra in S 2p region can be deconvoluted into two sets of peaks, indicating that S exists in two different chemical environments (Fig. 2b). Considering that Pt exists as Pt^{2+} and by comparison with pure $ZnIn_2S_4$, the peak at 161.39 and 162.64 eV can be assigned to S $2p_{3/2}$ and S $2p_{1/2}$ in $ZnIn_2S_4$, while the other two peaks at 160.84 and 162.08 eV can be assigned to S $2p_{3/2}$ and S $2p_{1/2}$ in PtS, respectively. It is known that the conduction band of hexagonal $ZnIn_2S_4$ located at –0.73 eV vs NHE, which is negative than $E(PtCl_6^{2-}/Pt^{2+})$ (0.21 V vs NHE). Therefore during the photoreduction process, the photogenerated electrons in $ZnIn_2S_4$ can reduce $PtCl_6^{2-}$ to surface adsorbed Pt^{2+}, which can further react with S^{2-} to form PtS, while CH_3OH act as sacrificial electron donor to consume the left photogenerated holes in $ZnIn_2S_4$ and complete the photocatalytic cycle. The photoreduction of $PtCl_6^{2-}$ over $ZnIn_2S_4$ to form surface deposited PtS for photocatalytic hydrogen evolution has also been reported previously [43]. The high resolution XPS spectra show peaks at 1021.65 and 1044.8 eV for Zn $2p_{3/2}$ and Zn $2p_{1/2}$, while peaks at 444.61 and 452.17 eV correspond to In $3d_{5/2}$ and In $3d_{3/2}$ (Fig. 2c and d). In comparison with those in bare $ZnIn_2S_4$ (Fig. S1), both the Zn 2p peaks and In 3d peaks in $PtS/ZnIn_2S_4$
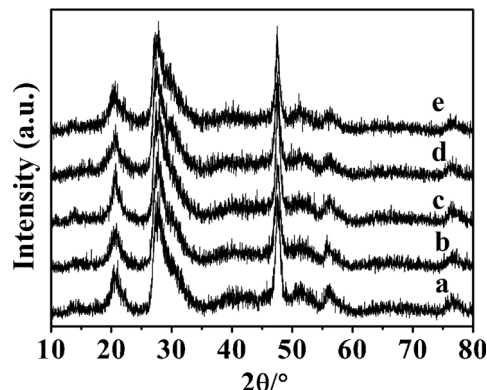

Fig. 1. Powder XRD of (a) $ZnIn_2S_4$; (b) 0.1 wt% $PtS/ZnIn_2S_4$; (c) 0.2 wt% $PtS/ZnIn_2S_4$; (d) 0.5 wt% $PtS/ZnIn_2S_4$; (e)1.0 wt% $PtS/ZnIn_2S_4$.
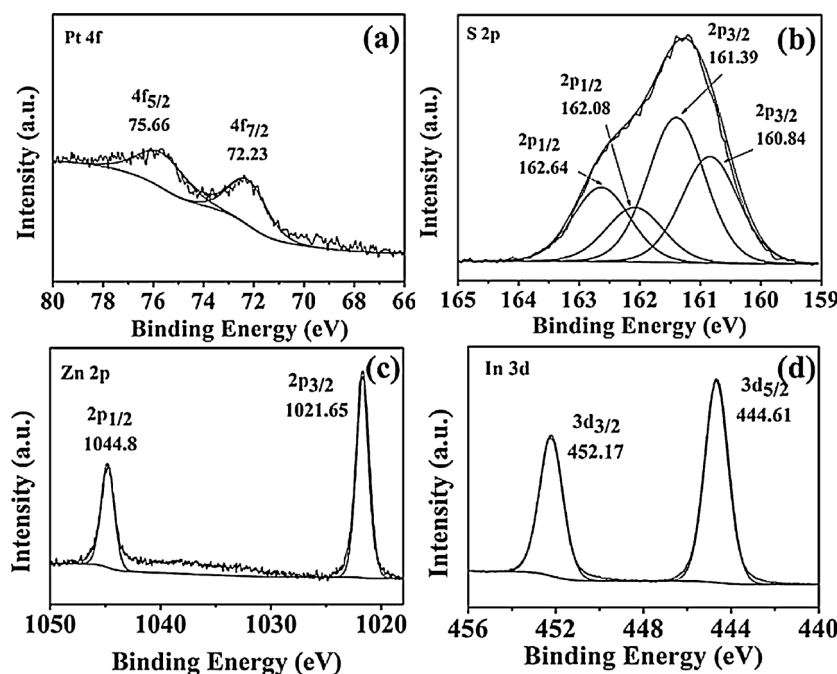
Fig. 2. XPS spectra of 0.5 wt% PtS/ZnIn$_2$S$_4$ (a) Pt 4f ; (b) S 2p; (c) Zn 2p and (d) In 3d.

shift to higher binding energies, indicating the existence of interaction between PtS and ZnIn$_2$S$_4$.

The SEM and TEM images of 0.5 wt% PtS/ZnIn$_2$S$_4$ nanocomposite show that the product is composed of flower-like microspheres with dimension in the range of 1–3 μm assembled by packed thin layers. It is clearly that the morphology of ZnIn$_2$S$_4$ is not significantly changed after the deposition of PtS (Fig. 3a and b). The HRTEM image shows nanoparticles with size of ca. 3 nm is deposited on ZnIn$_2$S$_4$ nanosheets. Besides clear lattice fringes of 0.325 nm ascribable to the (102) plane of hexagonal ZnIn$_2$S$_4$, clear lattice of 0.302 nm, which can be assigned to the (101) plane of PtS is also observed (Fig. 3c). This again confirms the presence of PtS nanoparticles in 0.5 wt% PtS/ZnIn$_2$S$_4$ nanocomposite.

The UV–vis DRS of PtS/ZnIn$_2$S$_4$ nanocomposites were displayed in Fig. 4. Although the loading of PtS onto ZnIn$_2$S$_4$ does not change the band gap of ZnIn$_2$S$_4$, the resultant PtS/ZnIn$_2$S$_4$ nanocomposites show enhanced absorption in the visible light region from 420 to 620 nm, in agreement with their khaki color.

The photocatalytic performance of PtS/ZnIn$_2$S$_4$ nanocomposites for the splitting of thiols to form disulfides in absence of oxidants was investigated under visible-light irradiation. The photocatalytic reaction was initially carried out with benzyl mercaptane as substrate in CH$_3$CN over 1.0 wt% PtS/ZnIn$_2$S$_4$ nanocomposite. 85% of benzyl mercaptane was transformed to dibenzyl disulfide after irradiated for 6 h, with almost quantitative amount of hydrogen generated (Table 1, entry 1). On the contrary, no dibenzyl disulfide or hydrogen was detected when the
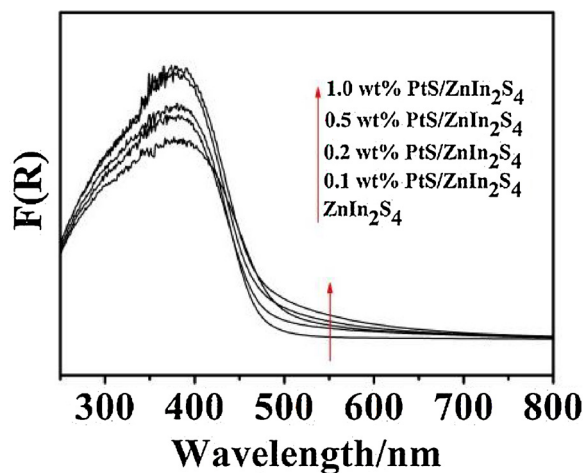

Fig. 4. UV–vis spectra of ZnIn$_2$S$_4$, 0.1 wt% PtS/ZnIn$_2$S$_4$, 0.2 wt% PtS/ZnIn$_2$S$_4$, 0.5 wt% PtS/ZnIn$_2$S$_4$ and 1.0 wt% PtS/ZnIn$_2$S$_4$.

reaction was carried out in absence of either light or PtS/ZnIn$_2$S$_4$, while only 48% of benzyl mercaptane was converted over bare ZnIn$_2$S$_4$ in 6 h (Table 1, entries 2–4). This indicates that the splitting of benzyl mercaptane to produce dibenzyl disulfide and hydrogen is actually induced by photocatalysis over ZnIn$_2$S$_4$, while PtS plays a promoting effect for
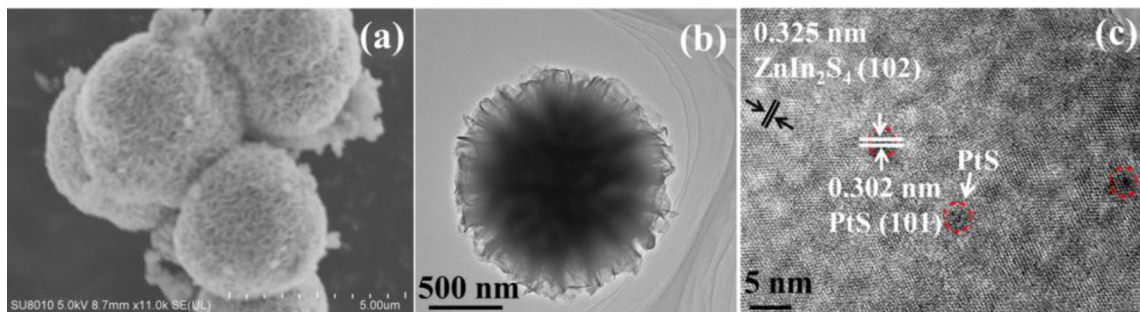

Fig. 3. 0.5 wt% PtS/ZnIn$_2$S$_4$ (a) SEM image; (b) TEM image; (c) HRTEM image.

Table 1
Photocatalytic conversion of benzyl mercaptane to produce dibenzyl disulfide and hydrogen under different conditions.

| Entry	Catalyst	Solvent	Conv. (%)[b]	Selec. (%)	Yield of H$_2$ (%)[c]
1	1.0 wt% PtS/ZnIn$_2$S$_4$	CH$_3$CN	85	> 99	85
2[d]	1.0 wt% PtS/ZnIn$_2$S$_4$	CH$_3$CN	ND	> 99	ND
3[e]	-	CH$_3$CN	ND	> 99	ND
4	ZnIn$_2$S$_4$	CH$_3$CN	48	> 99	36
5	1.0 wt% PtS/ZnIn$_2$S$_4$	Toluene	43	> 99	43
6	1.0 wt% PtS/ZnIn$_2$S$_4$	H$_2$O	17	> 99	17
7	1.0 wt% PtS/ZnIn$_2$S$_4$	EtOH/H$_2$O (3:1)	89	> 99	89
8	1.0 wt% PtS/ZnIn$_2$S$_4$	CH$_3$CN/H$_2$O (3:1)	95	> 99	95
9	0.1 wt% PtS/ZnIn$_2$S$_4$	CH$_3$CN/H$_2$O (3:1)	75	> 99	75
10	0.2 wt% PtS/ZnIn$_2$S$_4$	CH$_3$CN/H$_2$O (3:1)	84	> 99	84
11	0.5 wt% PtS/ZnIn$_2$S$_4$	CH$_3$CN/H$_2$O (3:1)	100	> 99	100
12[f]	0.5 wt% PtS/ZnIn$_2$S$_4$	CH$_3$CN/H$_2$O (3:1)	91	> 99	91

[a] Reaction conditions: Thiol (0.1 mmol), Catalyst (0.005 g), Solvent (2 ml), RT, under N$_2$ atmosphere, Visible light, Reaction time: 6 h; ND: not detected; [b] Determined by GC and GC/MS; [c] Determined by GC; [d] Without light; [e] No catalyst; [f] Thiol (0.5 mmol), Catalyst (0.01 g).

Fig. 5. The photocatalytic conversion of benzyl mercaptane and hydrogen generation over (1) 1.0 wt% Pd/ZnIn$_2$S$_4$; (2) 1.0 wt% MoS$_2$/ZnIn$_2$S$_4$; (3) 1.0 wt% NiS/ZnIn$_2$S$_4$; (4) 1.0 wt% PtS/ZnIn$_2$S$_4$ (reaction conditions: catalyst, 0.005 g; solvent (2 ml), CH$_3$CN/H$_2$O (3:1, v/v); reaction time, 6 h).

this reaction.

The solvent plays an important role in the photocatalytic splitting of benzyl mercaptane to form dibenzyl disulfide. Only 43% of benzyl mercaptane was converted in toluene and an even lower conversion (17%) of benzyl mercaptane was observed when water was used as the reaction medium under otherwise similar condition, probably due to the poor solubility of benzyl mercaptane in water (Table 1, entries 5 and 6). Among all the solvents investigated, a mixed solvent containing CH$_3$CN and H$_2$O in 3:1 (v/v) ratio gave the best performance by showing a superior conversion (95%) of benzyl mercaptane to produce dibenzyl disulfide in 6 h, with quantitative hydrogen produced in the meantime (Table 1, entry 8). Therefore, a mixed solvent of CH$_3$CN and H$_2$O (3:1, v/v) was chosen as the reaction medium for the following studies.

Since PtS plays a promoting role for photocatalytic splitting of thiols over ZnIn$_2$S$_4$, several other co-catalysts for hydrogen evolution, including transition metal chalcogenides MoS$_2$ and NiS as well as noble metal Pd, were also deposited on ZnIn$_2$S$_4$ and their performance for photocatalytic splitting of benzyl mercaptane was investigated (Fig. 5). As compared with bare ZnIn$_2$S$_4$, all the co-catalysts increased the conversion of benzyl mercapane over ZnIn$_2$S$_4$, but with different degree. In addition, quantitative hydrogen was only generated over MoS$_2$/ZnIn$_2$S$_4$ and PtS/ZnIn$_2$S$_4$ systems, indicating that the co-catalyst not only helps to increase the conversion of the benzyl mercaptane, but also is important for the concomitant generation of hydrogen.

The amount of deposited PtS also influences the photocatalytic activity for transformation of benzyl mercaptane. As indicated above, bare ZnIn$_2$S$_4$ show a poor activity, with only 48% of benzyl mercaptane converted in 6 h. In addition, less than quantitative of hydrogen was produced over bare ZnIn$_2$S$_4$. The introduction of only a little amount of PtS (0.1 wt%) not only significantly increased the conversion of benzyl
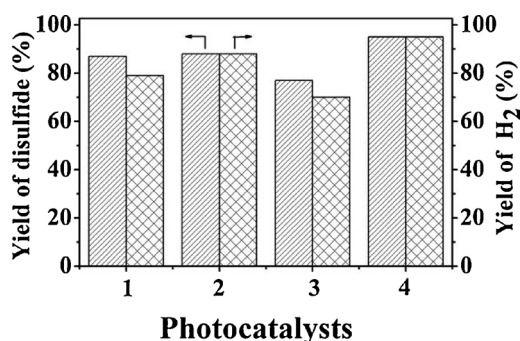
mercaptane to 75% in 6 h, but also led to quantitative production of hydrogen (Table 1, entry 9). Both the photocatalytic conversion of benzyl mercaptane and hydrogen generation increased with the deposited amount of PtS and an optimum PtS loading was found at 0.5 wt%, which completely converted benzyl mercaptane to form disulfide in 6 h (Table 1, entry 11). Further increase of the loading of PtS to 1.0 wt% resulted in a slightly decrease of the conversion of thiol (95%) in 6 h. The existence of an optimum loading amount for co-catalyst is frequently observed over semiconductor-based photocatalysts and is sometimes ascribed to the shading effect of co-catalyst, which blocks the absorption of the incident light by the semiconductors. The turnover number (TON) for the formation of dibenzyl disulfide in 6 h over 0.1 wt% PtS/ZnIn$_2$S$_4$ is calculated to be 2925 based on the amount of PtS, which is among the highest TON ever reported [12,13].

To elucidate the reaction mechanism, several control experiments were carried out. The addition of 0.5 equivalent of 2,2,6,6-tetra-methylpiperidine-1-oxyl (TEMPO), a radical scavenger, into the reaction system, led to a significantly decreased yield of 33% to the dibenzyl disulfide in otherwise similar reaction condition. This indicates that the radical is involved in the photocatalytic splitting of benzyl mercaptane to form dibenzyl disulfide over PtS/ZnIn$_2$S$_4$. This observation is in consistence with previous report on the photocatalytic transformation of thiols over CdSe QDs, in which the sulfenyl radicals were detected [13]. To study the origin of evolved hydrogen, D$_2$O was used in the reaction. However, unlike the photocatalytic splitting of benzyl mercaptane over CdSe QDs, which gave almost 100% of D$_2$ when H$_2$O was replaced by D$_2$O, a control reaction conducted in a mixture of CH$_3$CN and D$_2$O over PtS/ZnIn$_2$S$_4$ nanocomposite gave similar amount of dibenzyl disulfide with almost 100% H$_2$ instead of D$_2$. This result indicates that the hydrogen generated in the system comes from the photo splitting of thiol instead of H$_2$O.

Based on the above observations, a possible reaction mechanism for photocatalytic splitting of thiols to form disulfides over PtS/ZnIn$_2$S$_4$ nanocomposite was proposed (Scheme 1). First, thiols are adsorbed on the surface of ZnIn$_2$S$_4$. When irradiated with visible light, electrons and holes are generated over PtS/ZnIn$_2$S$_4$, in which photogenerated electrons are transferred to PtS nanoparticles. Since no obvious plasmonic peak assignable to PtS nanoparticles is observed in the DRS of the as-obtained PtS/ZnIn$_2$S$_4$ nanocomposites, the direct excitation of PtS to generate the "hot" electrons, as already evidenced in a variety of plasmonic nanocomposites, can be excluded [44]. The surface adsorbed RSH (RSH refers to thiols) can react with the photogenerated holes to produce sulfur-centered radicals (RS·), which can couple each other to form the corresponding disulfides. In the meantime, the reduction of proton occurs on PtS, which acts as the hydrogen evolution co-catalyst. The primary source of hydrogen comes from thiols instead of water, and almost no exchange of H$^+$ between H$_2$O and thiols occurs in our system as evidenced from the almost 100% of H$_2$ generated in D$_2$O medium.
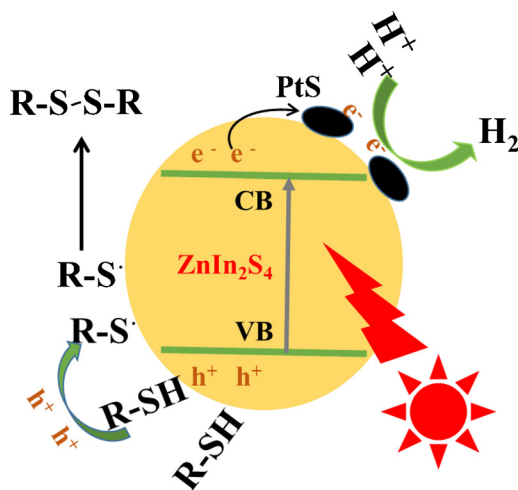
Scheme 1. Proposed mechanism for photocatalytic splitting of thiols to produce disulfides and hydrogen over PtS/ZnIn$_2$S$_4$ under visible light irradiation.
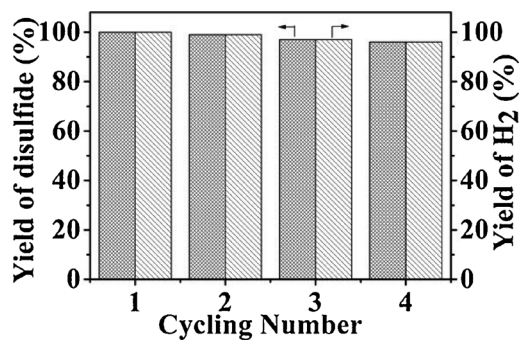
Table 2
Photocatalytic conversion of various thiols to disulfides over 0.5 wt% PtS/ZnIn$_2$S$_4$.

$$2\,RSH \xrightarrow[\text{hv, solvent, rt}]{\text{catalyst}} RS{-}SR + H_2$$

| Entry	Substrate	Time (h)	Conv. (%)[b]	Select. (%)	Yield of H$_2$ (%)[c]
1		6	96	97	96
2		6	97	> 99	97
3		6	98	96	98
4		6	100	> 99	100
5		5	99	> 99	100
6		5	93	95	93
7		5	97	94	97
8		6	71	94	71
9		6	78	97	78

[a] Reaction conditions: Thiol (0.1 mmol), Catalyst (0.005 g), Solvent (2 ml): CH$_3$CN/H$_2$O (3:1, v/v), RT, under N$_2$ atmosphere, Visible light; [b] Determined by GC and GC/MS; [c] Determined by GC.

Fig. 6. Cycling runs of photocatalytic splitting of benzyl mercaptane to produce dibenzyl disulfide and hydrogen over 0.5 wt% PtS/ZnIn$_2$S$_4$.
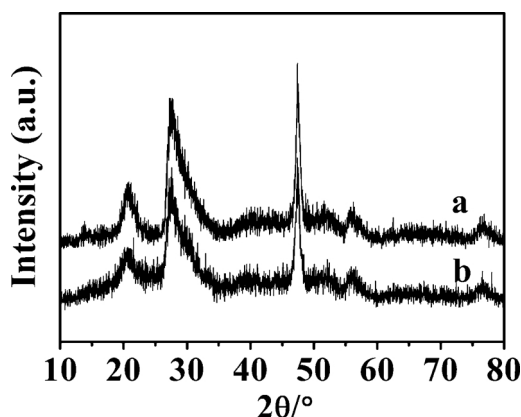
Fig. 7. Powder XRD of (a) fresh 0.5 wt% PtS/ZnIn$_2$S$_4$; (b) used 0.5 wt% PtS/ZnIn$_2$S$_4$ (after four cycling reactions).

This mechanism is clearly different from that previously observed over CdSe QDs, which shows a complete exchange of the H$^+$ between H$_2$O and thiols to produce D$_2$ when the reaction was carried out in D$_2$O.

The AQY for hydrogen generation over 0.5 wt% PtS/ZnIn$_2$S$_4$ nanocomposite was calculated to be 24.96% at 420 nm, which is among the highest value ever reported for ZnIn$_2$S$_4$ systems [45–47]. The high AQY of hydrogen generation over PtS/ZnIn$_2$S$_4$ nanocomposite can be ascribed to the simultaneous realization of the oxidation of thiols by the holes as well as the reduction of proton by the photogenerated electrons. The simultaneous consumption of photogenerated electrons and holes can effectively inhibit their recombination, which leads to a superior quantum efficiency.

The reaction protocol can also be applied in converting a broad range of thiols into their corresponding disulfides with good to excellent yield (71–100%). All benzyl mercaptanes with different substituents (Cl–, CH$_3$O–, and (CH$_3$)$_3$C–) on the phenyl ring, furfuryl mercaptan as well as thiophenols with different substituents on the phenol ring (CH$_3$– and NH$_2$–) show almost complete conversion in 5–6 h, indicating no clear electronic effect for this reaction (Table 2, entries 1–7). However, 2-naphthalenethiol and alicyclic thiol like cyclohexylthiol, show slightly lower conversion of 71% and 78% in 6 h, respectively, due to a steric effect (Table 2, entries 8 and 9).

PtS/ZnIn$_2$S$_4$ nanocomposites are stable during the photocatalytic splitting of thiols. Cycling tests showed that there was no obvious loss of the photocatalytic activity after four runs and the used PtS/ZnIn$_2$S$_4$ nanocomposite exhibited unchanged XRD spectrum after 4 cycling runs (Figs. 6 and 7). The reaction can also be scaled up by a factor of 5. A conversion of benzyl mercaptane conversion (91%) in 6 h with quantitative amount of hydrogen was still maintained over 0.5 wt% PtS/ZnIn$_2$S$_4$ (Table 1, entry 12).

4. Conclusions

In summary, small PtS nanoparticles were deposited on the surface of ZnIn$_2$S$_4$ via a photo reduction process and the resultant PtS/ZnIn$_2$S$_4$ nanocomposites show superior performance for photocatalytic splitting of thiols to produce disulfides with concomitant generation of hydrogen under visible light. The selective coupling of thiols over PtS/ZnIn$_2$S$_4$ can be carried out under mild condition and no over-oxidized products of thiols are obtained. PtS/ZnIn$_2$S$_4$ is stable during the reaction and can be easily separated for recycling. This study not only provides an

efficient and cost effective method for the production of disulfides, but also highlights the great potential of using semiconductor-based photocatalysts for light-driven organic syntheses.

Appendix A. Supplementary data

Supplementary material related to this article can be found, in the online version, at doi:https://doi.org/10.1016/j.apcatb.2018.04.030.

References

[1] F. Freeman, C.N. Angeletakis, J. Am. Chem. Soc. 105 (1983) 4039–4049.
[2] N. Iranpoor, D. Mohajer, A.-R. Rezaeifard, Tetrahedron Lett. 45 (2004) 3811–3815.
[3] M. Oba, K. Tanaka, K. Nishiyama, W. Ando, J. Org. Chem. 76 (2011) 4173–4177.
[4] Z. Zhang, W. Li, J. Liu, X. Chen, Y. Bu, J. Organomet. Chem. 706 (2012) 89–98.
[5] P.K. Dutta, A. Majumder, S. Dutta, B.B. Dhar, P. Munshi, S. Sen, Tetrahedron Lett. 58 (2017) 527–530.
[6] G. Delaittre, A.S. Goldmann, J.O. Mueller, C. BarnerKowollik, Angew. Chem. Int. Ed. 54 (2015) 11388–11403.
[7] H. Kisch, Angew. Chem. Int. Ed. 52 (2013) 812–847.
[8] G. Yang, D. Chen, H. Ding, J. Feng, J.Z. Zhang, Y. Zhu, S. Hamid, D.W. Bahnemannd, Appl. Catal. B: Environ. 219 (2017) 611–618.
[9] X. Lang, X. Chen, J. Zhao, Chem. Soc. Rev. 43 (2014) 473–486.
[10] X. Deng, Z. Li, H. García, Chem.-Eur. J. 23 (2017) 11189–11209.
[11] H.J. Kim, J.H. Yoon, S. Yoon, J. Phys. Chem. A 114 (2010) 12010–12015.
[12] K.Y.D. Tan, G.F. Teng, W.Y. Fan, Organometallics 30 (2011) 4136–4143.
[13] X.-B. Li, Z.-J. Li, Y.-J. Gao, Q.-Y. Meng, S. Yu, R.G. Weiss, C.-H. Tung, L.-Z. Wu, Angew. Chem. Int. Ed. 53 (2014) 2085–2089.
[14] P. Kumar, G. Singh, D. Tripathi, S.L. Jain, RSC Adv. 4 (2014) 50331–50337.
[15] D. Chauhan, P. Kumar, C. Joshi, N. Labhsetwar, S.K. Ganguly, S.L. Jain, New. J. Chem. 39 (2015) 6193–6200.
[16] Y. Chen, S. Hu, W. Liu, X. Chen, L. Wu, X. Wang, P. Liu, Z. Li, Dalton Trans. 40 (2011) 2607–2613.
[17] X. Jiao, Z. Chen, X. Li, Y. Sun, S. Gao, W. Yan, C. Wang, Q. Zhang, Y. Lin, Y. Luo, Y. Xie, J. Am. Chem. Soc. 139 (2017) 7586–7594.
[18] L. Ye, Z. Li, ChemCatChem 6 (2014) 2540–2543.
[19] X. Chen, S. Shen, L. Guo, S.S. Mao, Chem. Rev. 110 (2010) 6503–6570.
[20] Y. Chen, R. Huang, D. Chen, Y. Wang, W. Liu, X. Li, Z. Li, A.C.S. Appl, Mater. Inter. 4 (2012) 2273–2279.
[21] Y. Li, K. Zhang, S. Peng, G. Lu, S. Li, J. Mol. Catal. A: Chem. 363 (2012) 354–361.
[22] X. Zong, G. Wu, H. Yan, G. Ma, J. Shi, F. Wen, L. Wang, C. Li, Chem. Commun. 51 (2015) 2645–2648.
[23] Y.-J. Yuan, J.-R. Tu, Z.-J. Ye, D.-Q. Chen, B. Hu, Y.-W. Huang, T.-T. Chen, D.-P. Cao, Z.-T. Yu, Z.-G. Zou, Appl. Catal. B: Environ. 188 (2016) 13–22.
[24] L. Wei, Y. Chen, J. Zhao, Z. Li, Beilstein J. Nanotech. 4 (2013) 949–955.
[25] J. Zhou, G. Tian, Y. Chen, X. Meng, Y. Shi, X. Cao, K. Pan, H. Fu, Chem. Commun. 49 (2013) 2237–2239.
[26] Y. Chen, H. Ge, L. Wei, Z. Li, R. Yuan, P. Liu, X. Fu, Catal. Sci. Technol. 3 (2013) 1712–1717.
[27] J. Wang, Y. Chen, W. Zhou, G. Tian, Y. Xiao, H. Fu, H. Fu, J. Mater. Chem. A 5 (2017) 8451–8460.
[28] S. Shen, J. Chen, X. Wang, L. Zhao, L. Guo, J. Power Sources 196 (2011) 10112–10119.
[29] Z. Lei, W. You, M. Liu, G. Zhou, T. Takata, M. Hara, K. Domen, C. Li, Chem. Commun. 17 (2003) 2142–2143.
[30] L. Shang, C. Zhou, T. Bian, H. Yu, L.-Z. Wu, C.-H. Tung, T. Zhang, J. Mater. Chem. A 1 (2013) 4552–4558.
[31] N.S. Chaudhari, A.P. Bhirud, R.S. Sonawane, L.K. Nikam, S.S. Warule, V.H. Rane, B.B. Kale, Green. Chem. 13 (2011) 2500–2506.
[32] L. Ye, Z. Li, Appl. Catal. B: Environ. 160 (2014) 552–557.
[33] Q. Xiang, J. Yu, M. Jaroniec, J. Am. Chem. Soc. 134 (2012) 6575–6578.
[34] L. Wei, Y. Chen, Y. Lin, H. Wu, R. Yuan, Z. Li, Appl. Catal. B: Environ. 144 (2014) 521–527.
[35] X. Zong, X. Han, G. Ma, H. Yan, G. Wu, C. Li, J. Phys. Chem. C 115 (2011) 12202–12208.
[36] M.A. Lukowski, A.S. Daniel, C.R. English, F. Meng, A. Forticaux, R.J. Hamers, S. Jin, Energy Environ. Sci. 7 (2014) 2608–2613.
[37] W. Zhang, Y. Wang, Z. Wang, Z. Zhong, R. Xu, Chem. Commun. 46 (2010) 7631–7633.
[38] J. Ran, J. Zhang, J. Yu, M. Jaroniec, S.Z. Qiao, Chem. Soc. Rev. 43 (2014) 7787–7812.
[39] W. Zhang, J. Hong, J. Zheng, Z. Huang, J. Zhou, R. Xu, J. Am. Chem. Soc. 133 (2011) 20680–20683.
[40] Z. Wang, J. Peng, X. Feng, Z. Ding, Z. Li, Catal. Sci. Technol. 7 (2017) 2524–2530.
[41] Y. Zhu, Y. Xu, Y. Hou, Z. Ding, X. Wang, Int. J. Hydrogen Energy 39 (2014) 11873–11879.
[42] L. Ye, J. Fu, Z. Xu, R. Yuan, Z. Li, A.C.S. Appl, Mater. Inter. 6 (2014) 3483–3490.
[43] S. Wan, M. Ou, Q. Zhong, S. Zhang, F. Song, Chem. Eng. J. 325 (2017) 690–699.
[44] X.-C. Ma, Y. Dai, L. Yu, B.-B. Huang, Light-Sci Appl. 5 (2016) e16017.
[45] D. Zeng, L. Xiao, W.-J. Ong, P. Wu, H. Zheng, Y. Chen, D.-L. Peng, ChemSusChem 10 (2017) 4624–4631.
[46] B. Lin, H. Li, H. An, W. Hao, J. Wei, Y. Dai, C. Ma, G. Yang, Appl. Catal. B: Environ. 220 (2018) 542–552.
[47] F. Tian, R. Zhu, J. Zhong, P. Wang, F. Ouyang, G. Cao, Int. J. Hydrogen Energy 41 (2016) 20156–20171.